

Collective Dynamics in Active Polar Polymer Assemblies

Hossein Vahid,¹ Jens-Uwe Sommer,^{1,2,*} and Abhinav Sharma^{3,1,†}

¹Leibniz-Institut für Polymerforschung Dresden, Institut Theory der Polymere, 01069 Dresden, Germany

²Technische Universität Dresden, Institut für Theoretische Physik, 01069 Dresden, Germany

³Faculty of Mathematics, Natural Sciences, and Materials Engineering: Institute of Physics, University of Augsburg, Universitätsstraße 1, 86159 Augsburg, Germany

(Dated: March 17, 2025)

Active polymers respond to spatial activity gradients by autonomously migrating, a behavior central to biological self-organization and the design of intelligent synthetic materials. Using Brownian dynamics simulations, we investigate how the structure and propulsion direction of tangentially driven active polymers (TDAPs) determine their collective response to activity gradients. We show that TDAP assemblies exhibit strikingly different behaviors based on their organization: inward-directed arms form compact bundles that accumulate in low-activity regions, whereas outward-directed arms assemble into asters that undergo directed motion toward high-activity regions. Remarkably, mixed structures—comprising both inward- and outward-directed arms—display enhanced accumulation in the high-activity regions due to cooperative effects. Our results establish a fundamental link between polymer geometry and emergent transport, providing key design principles for programmable active materials.

Introduction.— Polymers are fundamental to biological systems, forming key structural and functional components across diverse cellular processes. These polymers typically self-organize into higher-order structures such as bundles, asters, and networks [1, 2]. These assemblies serve crucial functions: microtubule (MT) asters position centrosomes during mitosis [3–9], actin networks drive cellular migration [10–14], and filamentous bundles facilitate intracellular cargo transport [15]. Notably, many of these polymeric structures are active, driven far from equilibrium by molecular motors that exert forces along the polymer backbone [5, 16–21]. Inspired by biology, synthetic active systems have been designed to replicate and control such behaviors. Engineered MT asters [2, 22], actomyosin gels [5, 23], and colloidal self-assemblies [24–26] mimic biological functionality and respond to external signals such as light, magnetic fields, or chemical gradients.

Theoretical efforts to understand active biopolymers have extensively relied on tangentially driven active polymers (TDAPs) as model systems, capturing key features of motor-driven filaments in biological systems [27–33]. Studies of homogeneous activity landscapes have revealed diverse emergent behaviors, including polar ordering, clustered aggregates, and vortex states [34, 35]. While these studies have primarily focused on high-density regimes where interactions dominate, the role of activity gradients—ubiquitous in biological and synthetic environments [5, 23, 36–41]—remains largely unexplored.

In this Letter, we investigate the behavior of TDAPs in spatially varying activity landscapes. We demonstrate that while isolated TDAPs accumulate in low-activity regions, structured assemblies such as asters exhibit a qualitatively different response. Strikingly, we find that asters undergo directed motion, with their velocity and trajectory determined by their geometry and propulsion mech-

anism. Our results provide fundamental insight into the self-organization of active polymers in non-uniform environments, with direct implications for both biological systems and the design of responsive synthetic materials.

The model.—We perform Brownian dynamics simulations to investigate semiflexible TDAPs and multi-arm TDAPs (see Fig. 1(a)-(b)). Each TDAP bead experiences a self-propulsion force $\mathbf{F}_a^i = f_a \mathbf{e}^i$, where f_a is the magnitude of the active force, and \mathbf{e}^i denotes the unit vector indicating the propulsion direction. The propulsion direction of each bead (except for the polymer ends) at position \mathbf{r}^i is aligned with the local tangent vector of the polymer backbone, updated at each time step by $\mathbf{e}^i(t) = \mathbf{t}^i / |\mathbf{t}^i|$, where $\mathbf{t}^i = \mathbf{r}^{i-1} - \mathbf{r}^{i+1}$, and \mathbf{r}^{i-1} and \mathbf{r}^{i+1} represent the positions of the adjacent beads. For the first and last beads of the chains, \mathbf{e}^i aligns with the bond connecting them to their nearest neighbor bead.

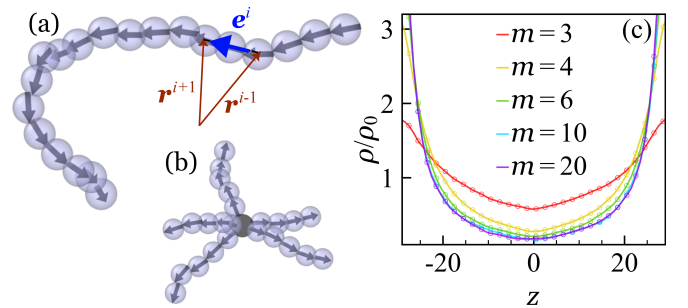


FIG. 1. Schematic representation of (a) a TDAP with $m = 20$, and (b) an aster with 5 arms, each having 5 beads. Arrows show the directions of self-propulsion forces. (c) Steady-state density of monomers along the z axis for varying m with $\rho_0 = 0.002$. Polymers are simple TDAPs as in (a), and the activity field is given by $f_a = 10(1 - |z|/30)$. TDAPs accumulate in the low-activity regions, and the accumulation is enhanced by increasing m .

The equation of motion of each bead is described by

$$\gamma_t \dot{\mathbf{r}}^i = - \sum_j \nabla_{\mathbf{r}^i} U^{ij} + \mathbf{F}_a^i + \boldsymbol{\xi}^i(t), \quad (1)$$

where γ_t is the translational friction coefficient of particle i , and U the potential energy. The stochastic noise $\boldsymbol{\xi}^i(t)$ is Gaussian, with zero mean $\langle \boldsymbol{\xi}^i(t) \rangle = 0$ and autocorrelation function $\langle \xi_\alpha^i(t) \cdot \xi_\beta^j(t') \rangle = 2\gamma_t^{-1} k_B T \delta_{\alpha\beta} \delta(t - t')$, where k_B is the Boltzmann constant, T the temperature, and $\alpha, \beta \in \{x, y, z\}$. Interparticle interactions are modeled using the Weeks-Chandler-Andersen (WCA) potential [42], $U_{\text{WCA}}^{ij}(r) = 4\epsilon [(\frac{\sigma^{ij}}{r^{ij}})^{12} - (\frac{\sigma^{ij}}{r^{ij}})^6 + \frac{1}{4}] \Theta(r_c^{ij} - r^{ij})$, where r^{ij} is the distance between particles i and j , and $\sigma^{ij} = 0.5(\sigma^i + \sigma^j)$ is their effective interaction diameter, with σ^i being the diameter of particle i . Here, ϵ is the depth of the potential well, Θ is the Heaviside step function, and the cutoff radius is set to $r_c^{ij} = 2^{1/6} \sigma^{ij}$.

In addition to WCA interactions, the bonded beads are connected using the finite extensible nonlinear elastic (FENE) potential [43], defined as $U_F(r) = -\frac{1}{2} k_F R_0^2 \ln[1 - (\frac{r^{ij}}{R_0})^2] \Theta(R_0 - r^{ij})$, where k_F represents the elastic coefficient and R_0 is the maximum bond length. The chain conformation is controlled by the bending potential $U_b = k_b [1 - \cos(\theta - \theta_0)]$, where k_b is the bending modulus, θ the angle between consecutive bonds, and θ_0 the rest angle.

We set $\sigma = 1$, $\epsilon = k_B T = 1$, and $\tau = \sigma^2 \gamma_t / (3k_B T)$, with $\gamma_t = 3$, as the units of length, energy, and time, respectively. All other physical quantities are measured in terms of these fundamental units. All simulations are conducted using the LAMMPS [44, 45] package within a cubic simulation box of dimensions $60 \times 60 \times 60 \sigma^3$, ranging from -30 to 30 along each axis. Periodic boundary conditions are imposed in all directions. The activity field varies linearly along the z -axis according to $f_a = f_a^*(1 - |z|/30)$, where $f_a = f_a^*$ at the box center $z = 0$, and $f_a = 0$ at $|z| = 30$. The systems studied contain N monodisperse chains, each with m monomers. The bulk density is defined as $\rho_0 = Nm/60^3$. The time step is set to $5 \times 10^{-4} \tau$. Each simulation runs for 2×10^8 steps, and the last 1.5×10^8 steps are used for data analysis. Steady-state density profiles of monomers along the z -axis are calculated as $\rho(z) = \langle n(t) \rangle_t / (60^2 \Delta z)$, where $\langle n(t) \rangle_t$ is the time-averaged number of beads within a slab of thickness $\Delta z = 0.6$ centered at position z . The simulation parameters are set to $\sigma^i = 1$, $k_F = 30$, $R_0 = 2\sigma^i$, $k_b = 30$, and $\theta_0 = 120^\circ$.

Results.—We first study individual TDAP chains. Fig. 1(c) shows these polymers tend to accumulate in the low-activity regions, and increasing the chain length m enhances their accumulation in those regions. TDAP propulsion aligns with the polymer backbone, and thus, longer TDAP chains preferentially orient and accumulate toward lower-activity regions. In contrast, active Brownian polymers (ABPOs) display length-dependent accu-

mulation and migrate toward the high-activity regions as the chain length m increases [46–48]; see Fig. S1 of the Supplementary Material (SM).

Individual TDAPs exhibit simple accumulation behavior; they migrate towards low activity regions. However, as we show below, when multiple TDAPs self-assemble into higher-order structures, they display markedly distinct accumulation dynamics. In many biological systems, active filaments are observed in assembled structures, such as bundles and asters [3, 4, 6–14]. Figure 2 shows that the directed motion and the overall conformation of two TDAPs connected to each other are significantly influenced by their relative propulsion directions. We connect two TDAP arms, each consisting of m' beads, to a central passive core. We consider two distinct activity orientations along the polymer backbone: inward-directed (tangential propulsion from the arm tips toward the core, Fig. 2(a)) and outward-directed (from the core toward the arm tips, Fig. 2(b)). In the inward-directed case, the two arms tend to approach each other, facilitating cooperative movement toward lower-activity regions. Inward propulsion creates effective inward-directed stresses leading to arm bending at the core position that stabilizes their collective migration toward low activity. Notably, variations in m' do not significantly influence this accumulation behavior.

In contrast, for outward-directed propulsion, the two arms exhibit a tug-of-war dynamic [49]. The tug-of-war of motor proteins was also found to be highly cooperative and perform directed cargo transport [50]. Here, propulsion forces stretch the polymer, and the polymer migrates toward high-activity regions. This occurs because when one arm aligns toward regions of higher activity, it experiences a stronger active force, pulling the entire polymer toward that region. It is consistent with previous studies on rigid dimers of ABPs, where outward-propelling dimers generate a net force leading to accumulation in high-activity regions, whereas inward-propelling dimers migrate toward low-activity regions [51]. As arm length

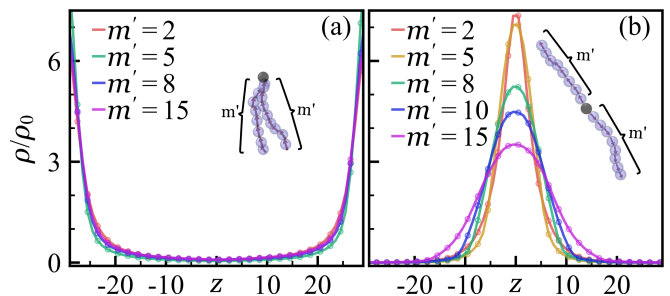


FIG. 2. Steady-state density of monomers along the z axis. Polymers have two symmetric TDAP arms, each containing m' monomers, connected to a passive core. (a) TDAPs are directed toward the core and accumulate in the low-activity regions. (b) TDAPs are directed away from the core and migrate to high-activity regions.

increases, monomers tend to accumulate in high-activity regions, but their spatial distribution becomes broader, and the peak density at the highest activity decreases. Since the polymer remains nearly stretched, not all beads can occupy the same z position. While the core remains in the high-activity region (see Fig. S4 of SM), the extended arms reach lower-activity areas. Furthermore, our results show that as the polymer becomes more stretched (increasing θ_0) or stiffer (increasing k_b), the accumulation in the high-activity regions enhances (cf. Fig. S5 of SM).

We next investigate how arm length asymmetry influences the accumulation behavior of such assemblies. In biological systems, cross-linked actin and microtubule structures often exhibit asymmetric arm lengths [23]. Our results show that when arm lengths are symmetric, the polymer strongly migrates toward regions of high activity. However, as asymmetry increases, this tendency reverses, leading to accumulation in low-activity regions. Interestingly, at intermediate asymmetry, the polymer density profile exhibits a distinctly bimodal shape, indicating coexistence or competition between arms to migrate to low- and high-activity regions. This transition suggests a delicate balance between pulling toward high and low activity regions (cf. Fig. S6 of SM).

Although the above results highlight the fundamental response of two-arm TDAPs to activity gradients, cytoskeletal networks and cellular assemblies often have more arms [52, 53]. In Fig. 3, findings for multi-arm polymers composed, each containing a fixed number of monomers ($m' = 5$), extending from a central passive core, are presented. We examine two distinct activity orientations: inward-directed propulsion (toward the central core, Fig. 3(a)) and outward-directed propulsion (away from the core, Fig. 3(b)). For inward-directed propulsion, the active arms tend to collapse close to each other, forming compact, bundle-like structures. These arms cooperatively move toward the low-activity region, and increasing the number of arms enhances accumulation in that region.

In contrast, outward-directed propulsion leads to open radial structures, resembling asters. In this case, asters accumulate in the high-activity regions. The accumulation displays nonmonotonic behavior with respect to the number of arms. Maximum accumulation in the high-activity region is achieved for the simplest two-arm structure, which decreases dramatically when a third arm is added. Here, the three-arm polymer faces competition among arms oriented toward different activity levels, reducing the net directional migration. Increasing the number of arms to four slightly improves accumulation relative to the three-arm structure. Further increases in arm number have minimal effects. These trends persist across different activity magnitudes (f_a^*) and bulk densities (ρ_0) (see Fig. S8 the SM). At high densities, accumulation extends to lower activity regions because of saturation effects in high-activity areas; however, the density peak

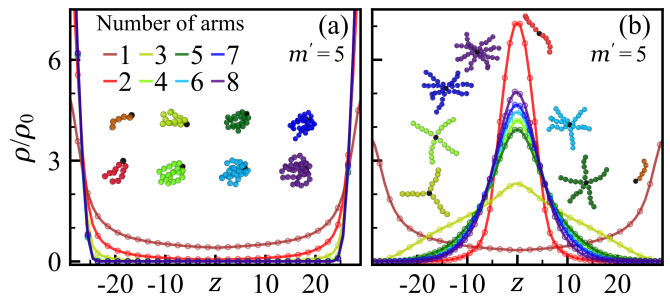


FIG. 3. Steady-state density of monomers along the z axis for polymers with varying numbers of arms. Each arm is an (a) inward- or (b) outward-directed TDAP with 5 monomers. The activity field is given by $f_a = 10(1 - |z|/30)$, and the bulk bead density is set to $\rho_0 = 0.002$. Inward-pointing TDAPs migrate to low-activity regions, whereas outwards-pointing ones migrate to high-activity regions.

remains in regions of highest activity.

Experiments demonstrated that inward- and outward-directed forces can be controlled using light-switchable motors [54] and by balancing motor forces with polymerization-driven expansion [23]. Additionally, layered asters can form in active MT-actin composites, where kinesin-driven MTs act as active arms, while actin filaments remain passive [55]. In Fig. 4(a), we examine polymers consisting of a varying number of passive arms (l) and $8 - l$ outward-directed TDAP arms, each with $m' = 5$ monomers. Increasing the number of passive arms from $l = 0$ to $l = 5$ progressively reduces aster accumulation in high-activity regions. Remarkably, at $l = 6$, where exactly two active TDAP arms remain, the polymer exhibits maximum accumulation in the high-activity region, consistent with our previous observation (Fig. 3(b)) for two-arm polymers. Increasing the number of passive arms to $l = 7$ reverses the behavior, resulting in accumulation in low-activity regions. Panel (b) shows the behavior of polymers with mixed propulsion directions: l inward-directed TDAP arms (toward the core) and $8 - l$ outward-directed TDAP arms (away from the core). Increasing the number of inward-directed arms from $l = 0$ to $l = 4$ reduces accumulation in the high-activity regions, with the minimal accumulation observed at $l = 5$, where three outward-directed arms compete strongly, resembling the reduced accumulation observed in three-arm asters (Fig. 3(b)). Surprisingly, at $l = 6$, with exactly two outward-directed TDAP arms, accumulation in high-activity regions is significantly enhanced. Here, the inward-directed arms cooperatively assist the two outward-directed arms, enabling strong collective migration toward high-activity regions. For $l > 6$, polymers migrate to low-activity regions.

A characteristic of biopolymer assemblies is that they are transient structures that can disassemble into single filaments [9, 18, 19, 38, 56–61]. For example, actin filaments are temporarily cross-linked and reorga-

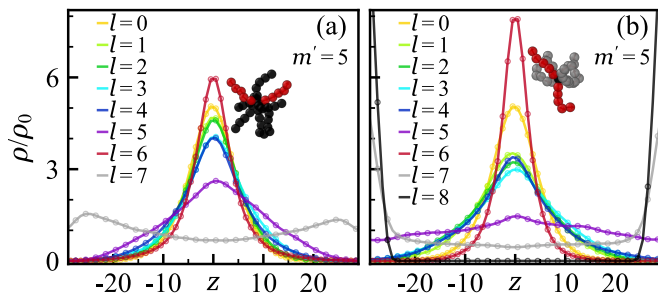


FIG. 4. Steady-state density of monomers along the z axis. Polymers have 8 arms, each with 5 monomers. (a) l arms are passive, and $8 - l$ arms are outward-directed TDAPs. (b) l arms are inward-directed TDAPs, and $8 - l$ arms are outward-directed TDAPs. The activity field is given by $f_a = 10(1 - |z|/30)$, and the bulk bead density is set to $\rho_0 = 0.002$. Accumulation in the high-activity regions decreases as the number of passive or inward-directed arms increases to 5. Accumulation in the high-activity regions is significantly enhanced at $l = 6$.

nized through the activity of molecular motors such as myosin [62, 63] or buckling [64]. A recent experiment demonstrated that plus-end-directed KIF11 motors facilitate MT plus-end bundling and minus-end-directed HSET motors stabilize bundles at low concentrations but induce transitions to asters at higher concentrations [18]. Inspired by this, we perform simulations for TDAPs with 5 monomers, each pulling a passive and attractive particle connected to the tail. The active force of the TDAPs is along their head. Polymers are confined within a spherical cell of radius $r = 30$. The activity increases toward the cortex as $f_a = 5r/30$. TDAP monomers interact via the WCA potential with other TDAP monomers and passive particles, whereas passive-passive interactions are described by the Lennard-Jones potential with an interaction well depth of ε (see Eq. (S3) of SM). The cortex is modeled as a spherical boundary at $r = 32.5$, interacting with all monomers and passive particles via a purely repulsive harmonic potential $E = 4(r - r_c)^2$ for $r < r_c$, where r is their distance from the cortex, and $r_c = 2.5\sigma$ defines the interaction range, beyond which the potential is zero. At weak attraction strengths ($\varepsilon < 10$), active forces dominate and prevent stable assemblies; thus, they accumulate in low-activity regions (center of the sphere). At $\varepsilon \approx 10$, asters form and migrate towards higher activity regions, but before reaching the cortex at $r \approx 17$, the active forces dominate and disassemble the asters. However, at $\varepsilon = 15$, the attraction is strong enough to maintain stable asters migrating to the cortex and accumulating there.

Finally, we examine the robustness of our findings by systematically varying key parameters, including polymer conformation, the strength and shape of the activity gradient, and partial activation of polymers (see SM). Across these variations, our results remain consistent,

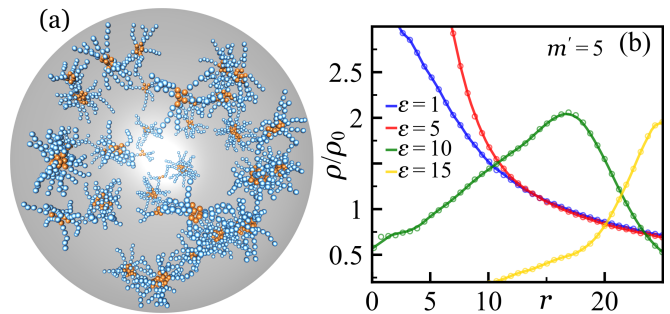


FIG. 5. (a) A simulation snapshot of 400 TDAPs, each with $m = 5$ (blue) pulling a passive attractive particle (orange). The polymers are confined in a spherical shell with radius $r = 30$. The activity field is given by $f_a = 5r/30$, and $\varepsilon = 15$. Polymers form asters and migrate toward the high-activity regions. (b) Steady-state density of monomers as a function of r for varying passive-passive attraction strength ε . At low ε , asters do not form, and polymers accumulate in low-activity regions. At $\varepsilon = 10$, asters form and migrate toward high-activity regions but disassemble at $r \approx 17$. At $\varepsilon = 15$, stable asters migrate and accumulate at the cortex.

demonstrating the generality of the observed behaviors.

In conclusion, assembling TDAPs into multi-arm structures alters their response to activity gradients. Propulsion direction determines where they migrate to and accumulate: one-end attached and inward-directed TDAPs form bundle-like structures accumulating in low-activity regions, while outward-directed TDAPs form aster-like structures migrating toward high-activity areas, with peaks observed for two-arm configurations. Mixed structures with two outward-directed and multiple inward-directed arms cooperatively migrate toward high-activity regions, leading to enhanced accumulation in those regions. Our findings highlight the crucial interplay between polymer architecture, propulsion directionality, and collective organization in directing active matter. Our findings could be experimentally tested using synthetic swimmers [65], synthetic chains of magnetic colloidal beads, where external fields control their assembly and motion, similar to magnetic colloidal asters [26]. Additionally, light patterns and light-controlled motor activation have also been used to generate and transport MT [5, 54] and actin [23, 37] assemblies such as asters, providing a potential method to explore the dynamics and stability of asters in inhomogeneous activity fields. Future work could explore the role of hydrodynamic interactions, the effect of population density on response, and the behavior of TDAPs in interconnected networks.

Acknowledgements.—A.S. acknowledges support by the Deutsche Forschungsgemeinschaft (DFG) within Project No. SH 1275/5-1. J.U.S. thanks the cluster of excellence “Physics of Life” at TU Dresden for its support.

-
- * jens-uwe.sommer@tu-dresden.de
† abhinav.sharma@uni-a.de
- [1] Y. Vyborna, J.-C. Galas, and A. Estevez-Torres, *J. Am. Chem. Soc.* **143**, 20022 (2021).
 - [2] Q. Xie, X. Chen, T. Wu, T. Wang, Y. Cao, S. Granick, Y. Li, and L. Jiang, *Nat. Commun.* **10**, 4954 (2019).
 - [3] P. A. Nguyen, A. C. Groen, M. Loose, K. Ishihara, M. Wühr, C. M. Field, and T. J. Mitchison, *Science* **346**, 244 (2014).
 - [4] K. Ishihara, P. A. Nguyen, A. C. Groen, C. M. Field, and T. J. Mitchison, *Proc. Natl. Acad. Sci.* **111**, 17715 (2014).
 - [5] T. D. Ross, H. J. Lee, Z. Qu, R. A. Banks, R. Phillips, and M. Thomson, *Nature* **572**, 224 (2019).
 - [6] Z. Feng, A. Caballe, A. Wainman, S. Johnson, A. F. Haensele, M. A. Cottee, P. T. Conduit, S. M. Lea, and J. W. Raff, *Cell* **169**, 1078 (2017).
 - [7] J. B. Woodruff, B. F. Gomes, P. O. Widlund, J. Mahamid, A. Honigmann, and A. A. Hyman, *Cell* **169**, 1066 (2017).
 - [8] G. D. Gupta and L. Pelletier, *Curr. Biol.* **27**, R836 (2017).
 - [9] S. R. Norris, S. Jung, P. Singh, C. E. Strothman, A. L. Erwin, M. D. Ohi, M. Zanic, and R. Ohi, *Nat. Commun.* **9**, 2659 (2018).
 - [10] M. Soares e Silva, M. Depken, B. Stuhmann, M. Korsten, F. C. MacKintosh, and G. H. Koenderink, *Proc. Natl. Acad. Sci.* **108**, 9408 (2011).
 - [11] F. Huber, D. Strehle, and J. Käs, *Soft Matter* **8**, 931 (2012).
 - [12] M. Bovellan, Y. Romeo, M. Biro, A. Boden, P. Chugh, A. Yonis, M. Vaghela, M. Fritzsche, D. Moulding, R. Thorogate, *et al.*, *Curr. Biol.* **24**, 1628 (2014).
 - [13] M. Fritzsche, D. Li, H. Colin-York, V. Chang, E. Moeendarbary, J. Felce, E. Sezgin, G. Charras, E. Betzig, and C. Eggeling, *Nat. Commun.* **8**, 14347 (2017).
 - [14] H. Colin-York, D. Li, K. Korobchevskaya, V. T. Chang, E. Betzig, C. Eggeling, and M. Fritzsche, *Commun. Biol.* **2**, 93 (2019).
 - [15] H. Tanimoto, A. Kimura, and N. Minc, *J. Cell Biol.* **212**, 777 (2016).
 - [16] D. Chowdhury, *Physica A Stat. Mech. Appl.* **372**, 84 (2006).
 - [17] J. Roostalu, J. Rickman, C. Thomas, F. Nédélec, and T. Surrey, *Cell* **175**, 796 (2018).
 - [18] G. Henkin, W.-X. Chew, F. Nédélec, and T. Surrey, *Proc. Natl. Acad. Sci.* **119**, e2206398119 (2022).
 - [19] B. Najma, W.-S. Wei, A. Baskaran, P. J. Foster, and G. Duclos, *Proc. Natl. Acad. Sci.* **121**, e2300174121 (2024).
 - [20] R. Ananthakrishnan and A. Ehrlicher, *Int. J. Biol. Sci.* **3**, 303 (2007).
 - [21] M. Bornens, *Science* **335**, 422 (2012).
 - [22] T. Nitta, Y. Wang, Z. Du, K. Morishima, and Y. Hiratsuka, *Nat. Mater.* **20**, 1149 (2021).
 - [23] M. Schuppler, F. C. Keber, M. Kröger, and A. R. Bausch, *Nat. Commun.* **7**, 13120 (2016).
 - [24] M. N. Popescu, *Langmuir* **36**, 6861 (2020).
 - [25] J. H. Bahng, B. Yeom, Y. Wang, S. O. Tung, J. D. Hoff, and N. Kotov, *Nature* **517**, 596 (2015).
 - [26] A. Snezhko and I. S. Aranson, *Nat. Mater.* **10**, 698 (2011).
 - [27] V. Schaller, C. Weber, C. Semmrich, E. Frey, and A. R. Bausch, *Nature* **467**, 73 (2010).
 - [28] G. De Canio, E. Lauga, and R. E. Goldstein, *J. R. Soc. Interface* **14**, 20170491 (2017).
 - [29] S. K. Anand and S. P. Singh, *Phys. Rev. E* **98**, 042501 (2018).
 - [30] V. Bianco, E. Locatelli, and P. Malgaretti, *Phys. Rev. Lett.* **121**, 217802 (2018).
 - [31] C. A. Philipps, G. Gompper, and R. G. Winkler, *J. Chem. Phys.* **157** (2022).
 - [32] J.-X. Li, S. Wu, L.-L. Hao, Q.-L. Lei, and Y.-Q. Ma, *Phys. Rev. Res.* **5**, 043064 (2023).
 - [33] M. Fazlzadeh, E. Irani, Z. Mokhtari, and S. Jabbarifarouji, *Phys. Rev. E* **108**, 024606 (2023).
 - [34] C. Zhao, R. Yan, and N. Zhao, *J. Chem. Phys.* **161** (2024).
 - [35] R. E. Isele-Holder, J. Elgeti, and G. Gompper, *Soft matter* **11**, 7181 (2015).
 - [36] C. J. Miller, P. K. LaFosse, S. B. Asokan, J. M. Haugh, J. E. Bear, and T. C. Elston, *Integr. Biol.* **11**, 280 (2019).
 - [37] R. Zhang, S. A. Redford, P. V. Ruijgrok, N. Kumar, A. Mozaffari, S. Zemsky, A. R. Dinner, V. Vitelli, Z. Bryant, M. L. Gardel, *et al.*, *Nat. Mater.* **20**, 875 (2021).
 - [38] C. Hentrich and T. Surrey, *J. Cell Biol.* **189**, 465 (2010).
 - [39] S. Saha, R. Golestanian, and S. Ramaswamy, *Phys. Rev. E* **89**, 062316 (2014).
 - [40] J. Palacci, S. Sacanna, A. P. Steinberg, D. J. Pine, and P. M. Chaikin, *Science* **339**, 936 (2013).
 - [41] M. A. Ubertini, E. Locatelli, and A. Rosa, *ACS Macro Lett.* **13**, 1204 (2024).
 - [42] J. D. Weeks, D. Chandler, and H. C. Andersen, *J. Chem. Phys.* **54**, 5237 (1971).
 - [43] R. B. Bird, C. F. Curtiss, R. C. Armstrong, and O. Hassager, *Dynamics of polymeric liquids* (Wiley, New York, 1987).
 - [44] S. Plimpton, *J. Comput. Phys.* **117**, 1 (1995).
 - [45] A. P. Thompson, H. M. Aktulga, R. Berger, D. S. Bolintineanu, W. M. Brown, P. S. Crozier, P. I. Veld, A. Kohlmeyer, S. G. Moore, T. D. Nguyen, R. Shan, M. J. Stevens, J. Tranchida, C. Trott, and S. J. Plimpton, *Comp. Phys. Comm.* **271**, 108171 (2022).
 - [46] H. D. Vuijk, H. Merlitz, M. Lang, A. Sharma, and J.-U. Sommer, *Phys. Rev. Lett.* **126**, 208102 (2021).
 - [47] S. Ravichandir, B. Valecha, P. L. Muzzeddu, J.-U. Sommer, and A. Sharma, *Soft Matter* **21**, 1835 (2025).
 - [48] P. L. Muzzeddu, A. Gambassi, J.-U. Sommer, and A. Sharma, *Phys. Rev. Lett.* **133**, 118102 (2024).
 - [49] P. L. Muzzeddu, H. D. Vuijk, H. Löwen, J.-U. Sommer, and A. Sharma, *J. Chem. Phys.* **157** (2022).
 - [50] M. J. Müller, S. Klumpp, and R. Lipowsky, *Proc. Natl. Acad. Sci.* **105**, 4609 (2008).
 - [51] H. D. Vuijk, S. Klempahn, H. Merlitz, J.-U. Sommer, and A. Sharma, *Phys. Rev. E* **106**, 014617 (2022).
 - [52] C. A. Weber, R. Suzuki, V. Schaller, I. S. Aranson, A. R. Bausch, and E. Frey, *Proc. Natl. Acad. Sci.* **112**, 10703 (2015).
 - [53] C. P. Brangwynne, G. H. Koenderink, F. C. MacKintosh, and D. A. Weitz, *J. Cell Biol.* **183**, 583 (2008).
 - [54] L. M. Lemma, M. Varghese, T. D. Ross, M. Thomson, A. Baskaran, and Z. Dogic, *PNAS nexus* **2**, pgad130 (2023).
 - [55] J. Berezney, B. L. Goode, S. Fraden, and Z. Dogic, *Proc. Natl. Acad. Sci.* **119**, e2115895119 (2022).

- [56] D. Gordon, A. Bernheim-Groswasser, C. Keasar, and O. Farago, *Phys. Biol.* **9**, 026005 (2012).
- [57] M. E. Tanenbaum, R. D. Vale, and R. J. McKenney, *Elife* **2**, e00943 (2013).
- [58] T. H. Tan, M. Malik-Garbi, E. Abu-Shah, J. Li, A. Sharma, F. C. MacKintosh, K. Keren, C. F. Schmidt, and N. Fakhri, *Sci. Adv.* **4**, eaar2847 (2018).
- [59] C. Utzschneider, B. Suresh, A. Sciortino, J. Gaillard, A. Schaeffer, S. Pattanayak, J.-F. Joanny, L. Blanchoin, and M. Théry, *Proc. Natl. Acad. Sci.* **121**, e2406985121 (2024).
- [60] A. Lamtyugina, D. S. Banerjee, Y. Qiu, and S. Vaikuntanathan, *bioRxiv*, 2024 (2024).
- [61] B. Lemma, N. P. Mitchell, R. Subramanian, D. J. Needle-

- man, and Z. Dogic, *Phys. Rev. X.* **12**, 031006 (2022).
- [62] J. Prost, F. Jülicher, and J.-F. Joanny, *Nat. Phys.* **11**, 111 (2015).
- [63] Y. H. Tee, T. Shemesh, V. Thiagarajan, R. F. Hariadi, K. L. Anderson, C. Page, N. Volkmann, D. Hanein, S. Sivaramakrishnan, M. M. Kozlov, *et al.*, *Nat. Cell Biol.* **17**, 445 (2015).
- [64] K. Matsuda, W. Jung, Y. Sato, T. Kobayashi, M. Yamagishi, T. Kim, and J. Yajima, *Cytoskeleton* **81**, 339 (2024).
- [65] Y. Ji, X. Lin, Z. Wu, Y. Wu, W. Gao, and Q. He, *Angew. Chem.* **131**, 12328 (2019).

Supplemental Material for

Collective Dynamics in Active Polar Polymer Assemblies

ACTIVE BROWNIAN POLYMERS

For active Brownian particles (ABPs), the orientation \mathbf{e}^i of the self-propulsion force is different from that of tangentially driven active polymers (TDAPs), and it is given by

$$\dot{\mathbf{e}}^i(t) = \boldsymbol{\eta}^i(t) \times \mathbf{e}^i(t), \quad (\text{S1})$$

where $\boldsymbol{\eta}$ is a Gaussian white noise that has $\langle \boldsymbol{\eta}^i(t) \rangle = 0$ and $\langle \boldsymbol{\eta}^i(t) \cdot \boldsymbol{\eta}^j(t') \rangle = 2k_B T \gamma_r^{-1} \delta^{ij} \delta(t - t')$, with γ_r as the rotational friction coefficient. We set the rotational friction coefficient for ABPs as $\gamma_r = \gamma_t \sigma^2 / 3$.

Figure S1 shows that with increasing the number of monomers m , active Brownian polymers (ABPOs) accumulate in high-activity regions, which is further enhanced by increasing m . However, as discussed in the main paper, TDAPs accumulate in low-activity regions, which is enhanced with increasing m .

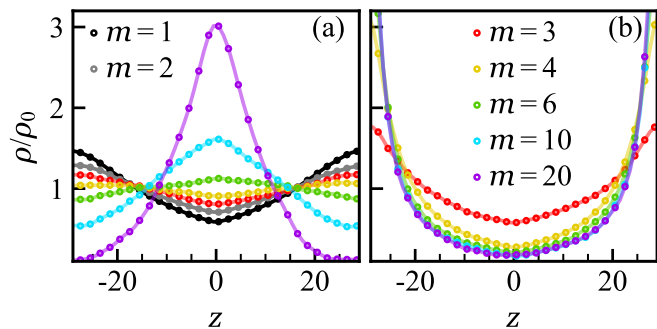


FIG. S1. Steady state density of polymer beads along the z axis for (a) ABPOs and (b) TDAPs. Polymers have m beads and $\rho_0 = 0.002$. The activity field is given by $f_a = 10(1 - |z|/30)$.

EFFECT OF TDAP'S HEAD MONOMER ACTIVITY

We change the activity of the head monomer of a TDAP. Figure S2 presents the results for TDAPs connected to a passive monomer, an ABP, or a tangent monomer. There is no significant difference between the case where the head is passive or tangent. However, the accumulation in low-activity regions is slightly enhanced when the head monomer is an ABP.

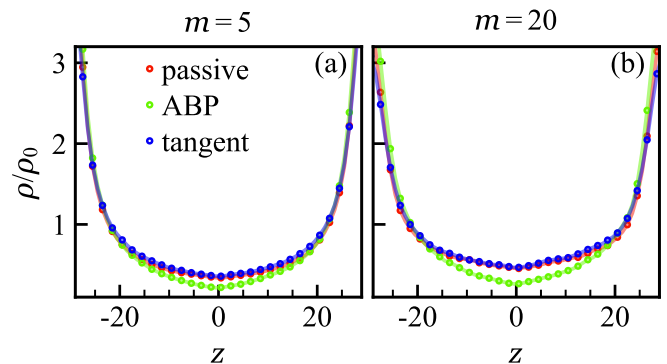


FIG. S2. Steady state density of TDAP beads along the z axis for (a) $m = 5$ and (b) $m = 20$. The head monomer is either passive, an ABP, or tangent (along the bond). The bulk density $\rho_0 = 0.002$, and the activity field is given by $f_a = 10(1 - |z|/30)$.

EFFECT OF POLYMER CONFORMATION

In Fig. S3, we vary the equilibrium angle θ_0 from 60° to 180° . As θ_0 increases from 60° to 120° , the accumulation of ABPOs in high-activity regions is increased, and the TDAP accumulation in the low-activity region is suppressed. For $\theta_0 > 120^\circ$, the polymer adopts an increasingly rod-like conformation, leading to a significant

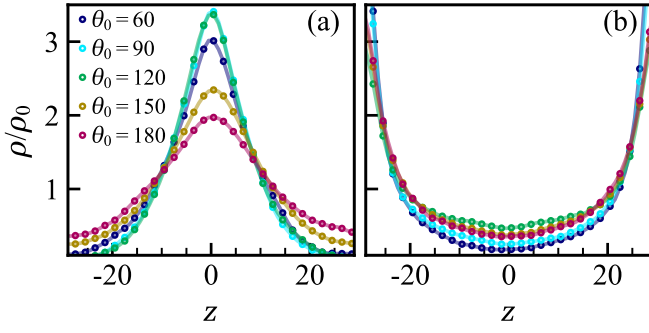


FIG. S3. Steady state density of polymer beads with $m = 20$ along the z axis for (a) ABPOs and (b) TDAPS for varying θ_0 (see Eq. (3) of the main manuscript). The bulk density $\rho_0 = 0.002$, and the activity field is given by $f_a = 10(1 - |z|/30)$.

reduction in ABPO accumulation in high-activity regions and an increase in TDAP in low-activity regions, as the steric constraints and propulsion alignment become more pronounced.

EFFECT OF ARM CHARACTERISTICS ON ACCUMULATION

In Fig.2(b) of the main manuscript, we show that two-arm polymer accumulation varies with arm length, where the normalized steady-state density of all monomers is calculated. Figure S4 presents the steady-state density of the polymer core. The minimum accumulation of core in the high-activity region is observed for $m' = 2$ and at $m' > 2$ the accumulation the high-activity region is enhanced, and increasing m' further does not have significant effects on the accumulation.

Moreover, in Fig. 2 of the main manuscript, we show that two-arm TDAPs accumulate in high-activity regions when the arms are propelled outward from the core to the tip and accumulate in low-activity regions when propelled inward from the tip to the core. To investigate

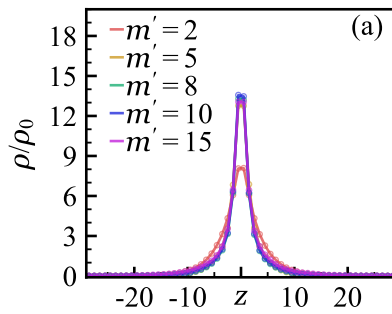


FIG. S4. Steady state density of the center of mass of two-arm polymers along the z . Arms are outward-directed and symmetric, each with m' monomers. The bulk density $\rho_0 = 0.002$, and the activity field is given by $f_a = 10(1 - |z|/30)$.

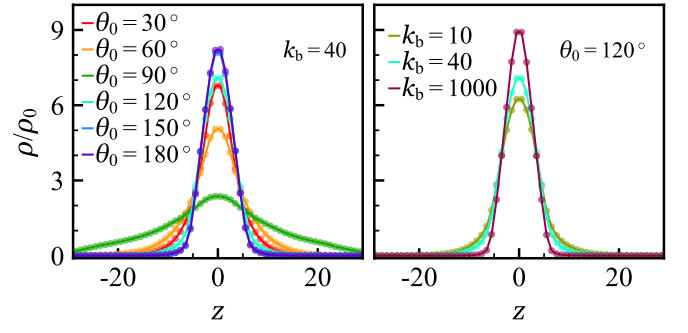


FIG. S5. Steady-state density distribution of beads of star-like TDAPs along the z axis for varying (a) θ_0 and (b) k_b . Polymers have two symmetric arms, each containing $m' = 5$ beads. The self-propulsion force on each bead of arms is toward the tip and tangent to the arm. The activity field is given by $f_a = 10(1 - |z|/30)$, and the bulk bead density is set to $\rho_0 = 0.002$.

the effects of conformation and rigidity on accumulation, we vary θ_0 and k_b . As θ_0 and k_b increase, the polymer becomes more stretched and rigid, respectively, leading to enhanced accumulation in high-activity regions (see Fig. S5). This effect arises because the tug-of-war between the arms intensifies, increasing the net propulsion toward higher activity regions.

Figure S6(a) presents the results for polymers consisting of a passive core and two asymmetric TDAP arms. The total number of active beads is fixed at 20, and we vary the fraction x , defined as the length ratio between the shorter and longer arms (see schematic in Fig. S6(a)). The polymer exhibits strong accumulation in high-activity regions when the arms are symmetric ($x = 0.5$). However, as the arms become increasingly asymmetric (decreasing x), the polymers gradually migrate to low-activity regions and accumulate in low-activity regions. This accumulation response becomes prominent in extreme asymmetry ($x < 0.2$). Interest-

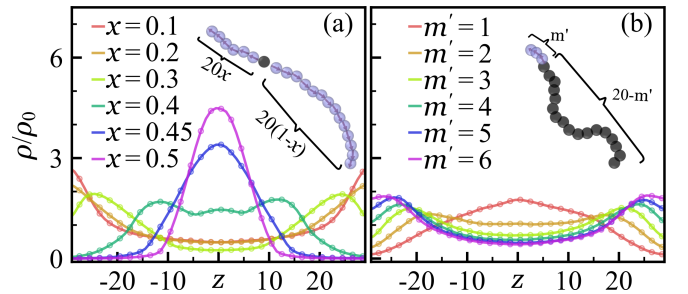


FIG. S6. Steady state density of two-arm polymer beads along the z . (a) Arms are outward-directed and asymmetric, with one having $20x$ and the other one $20(1-x)$ beads. (b) A pulling TDAP with m' monomer connected to a passive polymer with $20 - m'$ beads. The bulk density $\rho_0 = 0.002$, and the activity field is given by $f_a = 10(1 - |z|/30)$.

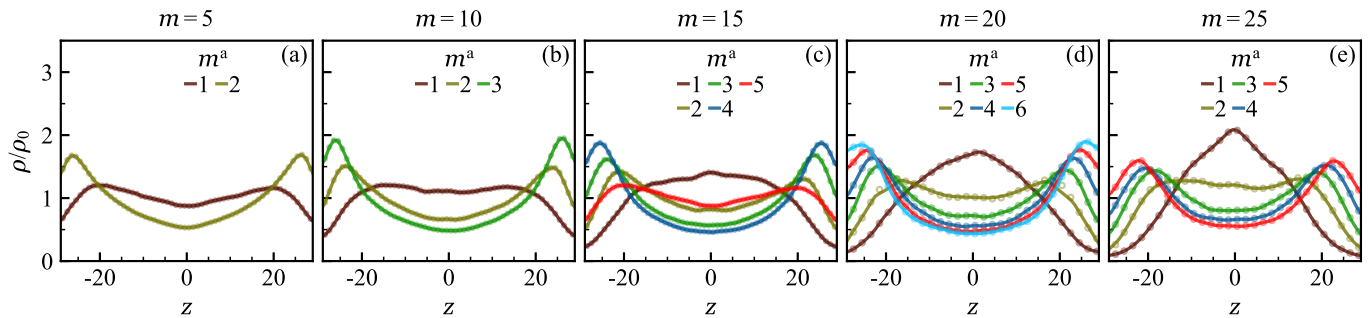


FIG. S7. Steady state density of two-arm polymer beads along the z . A pulling TDAP with m^a monomer connected to a passive polymer. The total number of polymer monomers is m . The bulk density $\rho_0 = 0.002$, and the activity field is given by $f_a = 10(1 - |z|/30)$.

ingly, at intermediate asymmetry ($x \approx 0.4$), the polymer density profile exhibits a distinctly bimodal shape, indicating coexistence or competition between arms to migrate toward low and high-activity regions. This transition suggests a delicate balance between pulling toward these regions, which arises from the asymmetric propulsion of the two arms, causing the polymer to fluctuate between these two regions. For additional results exploring chain lengths other than 20 active beads, see Fig. S5 of SM.

In Fig. S6(b), the polymer consists of a passive segment pulled by an active TDAP. The polymer has a fixed total length of 20 beads, and we vary the number of active beads (m') at one end. For $m' = 1$, the polymers accumulate modestly in high-activity regions. As m' increases, we observe the formation of distinctly bimodal density profiles. This indicates that the polymer spends comparable amounts of time in both high- and low-activity regions, preferentially more time in the low-activity regions. We have performed additional simulations for polymers with varying total lengths m and the number of active monomers m^a pulling the passive segment (see Fig. S6). These show that short chains accumulate in low-activity regions, whereas longer chains $m > 15$ accumulate in high-activity regions. The latter is enhanced as the chain length increases.

EFFECT OF ACTIVITY GRADIENT AND ASTER DENSITY ON ASTER ACCUMULATION

In Fig. 3(b) of the main manuscript, we show that polymers accumulate in the high-activity regions when the propulsion of TDAPs forming a multi-arm aster is outward from the core to the tips. Figure S8(a) presents the results for multi-arm polymers in an activity gradient given by $f_a = f_a^*(1 - |z|/30)$ for varying f_a^* . It shows that the accumulation of asters in the high activity region is robust and is not affected by f_a^* .

Additionally, as the number of asters in the simulation box increases, the accumulation in the high-activity re-

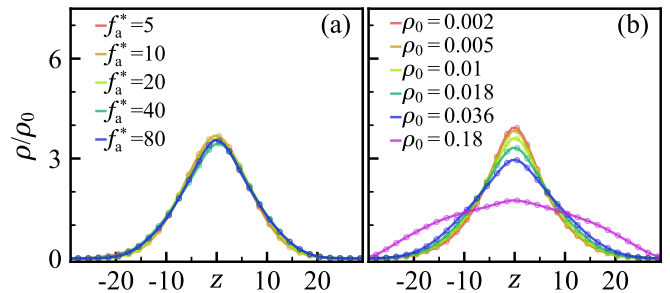


FIG. S8. (a) Steady-state density of aster-like polymer beads with each arm $m' = 10$ along the z . The bulk density $\rho_0 = 0.002$, and the activity field is given by $f_a = f_a^*(1 - |z|/30)$ for varying f_a^* . (b) Steady-state density of aster-like polymer beads with each arm $m' = 5$ along the z for varying bulk density ρ_0 . The activity field is given by $f_a = 10(1 - |z|/30)$.

gions decreases due to excluded volume effects. At higher densities, particles progressively saturate the highest activity regions, reducing the available space for further accumulation. Since these regions can only accommodate a limited number of asters without overlap, excess asters are displaced into adjacent lower-activity areas.

CONFINED TDAPS

We present the results for TDAPs connected to a passive and attractive bead in Fig. 5 of the main manuscript. The interactions of active particles are described by Eq. (1) of the main manuscript. The passive-passive bead interactions are described by the Lennard-Jones (LJ) potential

$$U_{LJ}^{ij}(r) = \begin{cases} 4\epsilon \left[\left(\frac{\sigma^{ij}}{r^{ij}} \right)^{12} - \left(\frac{\sigma^{ij}}{r^{ij}} \right)^6 \right], & r^{ij} < 2.5\sigma^{ij}; \\ 0, & \text{otherwise;} \end{cases} \quad (\text{S2})$$

where r^{ij} is the distance between the particles i and j , ϵ the depth of the potential well, and $\sigma^{ij} = 0.5(\sigma^i + \sigma^j)$ is their interaction diameter.